JACS
JOURNAL OF THE AMERICAN CHEMICAL SOCIETY
Article
pubs.acs.org/JACS

Direct Probing of the Structure and Electron Transfer of Fullerene/Ferrocene Hybrid on Au(111) Electrodes by in Situ Electrochemical STM

Ting Chen,[†] Dong Wang,*[,†] Li-Hua Gan,[§] Yutaka Matsuo,*[,‡] Jing-Ying Gu,[†,∥] Hui-Juan Yan,[†] Eiichi Nakamura,[‡] and Li-Jun Wan*[,†]

[†]Key Laboratory of Molecular Nanostructure and Nanotechnology and Beijing National Laboratory for Molecular Sciences, Institute of Chemistry, Chinese Academy of Sciences (CAS), Beijing 100190, People's Republic of China

[∥]University of CAS, Beijing 100049, People's Republic of China

[‡]Department of Chemistry, The University of Tokyo, 7-3-1 Hongo, Bunkyo-ku, Tokyo 113-0033, Japan

[§]School of Chemistry and Chemical Engineering, Southwest University, Chongqing 400715, People's Republic of China

Supporting Information

ABSTRACT: The electron donor–acceptor dyads are an emerging class of materials showing important applications in nonlinear optics, dye-sensitized solar cells, and molecular electronics. Investigation of their structure and electron transfer at the molecular level provides insights into the structure–property relationship and can benefit the design and preparation of electron donor–acceptor dyad materials. Herein, the interface adstructure and electron transfer of buckyferrocene Fe($C_{60}Me_5$)Cp, a typical electron donor–acceptor dyad, is directly probed using in situ electrochemical scanning tunneling microscopy (STM) combined with theoretical simulations. It is found that the adsorption geometry and assembled structure of Fe($C_{60}Me_5$)Cp is significantly affected by the electrochemical environments. In 0.1 M $HClO_4$ solution, Fe($C_{60}Me_5$)Cp forms well-ordered monolayers and multilayers on Au(111) surfaces with molecular dimer as the building block. In 0.1 M $NaClO_4$ solution, typical six-fold symmetric close-packed monolayer with vertically adsorbed Fe($C_{60}Me_5$)Cp is formed. Upon electrochemical oxidation, the oxidized Fe($C_{60}Me_5$)Cp shows higher brightness in an STM image, which facilitates the direct visualization of the interfacial electrochemical electron transfer process. Theoretical simulation indicates that the electrode potential-activated, one-electron transfer from Fe($C_{60}Me_5$)Cp to the electrode leads to the change of the delocalization character of the frontier orbital in the molecule, which is responsible for the STM image contrast change. This result is beneficial for understanding the structure and property of single electron donor–acceptor dyads. It also provides a direct approach to study the electron transfer of electron donor–acceptor compounds at the molecular level.

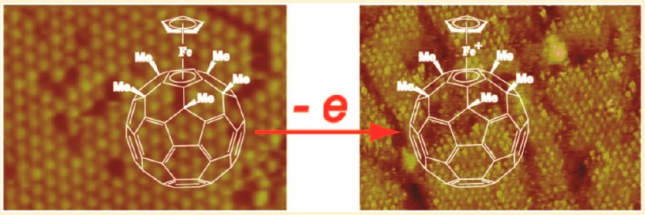

1. INTRODUCTION

The electron donor–acceptor conjugates, which undergo intramolecular charge transfer under external stimulus, have attracted increasing attention due to their outstanding optical and electronic properties and important applications in many fields including nonlinear optics, dye-sensitized solar cells, and molecular electronics.[1−7] Fullerene is one of the most widely used electron acceptor units in such compounds for its unique cage structure and small reorganization energy in electron transfer reactions.[8] A number of molecular dyads, triads, and tetrads of fullerenes covalently linked to an electron donor such as porphyrin, phthalocyanine, tetrathiafulvalene, ferrocene, and so on, have been synthesized and intensively studied.[3−6,9−15] These fullerene-donor linked compounds exhibit excellent photovoltaic effect upon photoirradiation.[16−19] Furthermore, enhancement of the nonlinear optical response was observed for fullerene dyads compared to that of pristine fullerenes.[10,11] Such functions can be attributed to the strong electron transfer behavior and the hyperpolorizability of the fullerene dyads linked with electron donors. Investigation of the structure and property of electron donor–acceptor dyads at the molecular level can benefit the understanding of their structure–function relationship and provides an experimental basis for the design and preparation of electron donor–acceptor dyad materials.

Scanning tunneling microscopy (STM) is a powerful technique to study the structure and property of single molecule on solid surfaces. It has been widely used to explore the molecular adsorption geometry and the assembled structures on surfaces.[20−22] Moreover, STM offers comprehensive information about the electronic properties of single molecules.[23] STM has been used to directly probe the charge localization within a single molecule of the mixed-valence complexes.[24,25] Ye et al. studied the electrochemically

Received: November 20, 2013
Published: January 31, 2014

   dx.doi.org/10.1021/ja411813r | J. Am. Chem. Soc. 2014, 136, 3184−3191

controlled single-molecule station changes within bistable rotaxane molecules by in situ STM.[26] Recently, Tsoi et al. described the reversible conductance switching in single quinone-modified oligo(phenylene vinylene) molecules using electrochemical STM. The switching is controlled by the electrochemical potential and is suggested to originate from the alteration of the electronic structure.[27] The charge transfer process, which is involved in many photo-electronic functional materials, can be characterized by STM, too. Jäckel et al. investigated the molecular charge transfer inside an electron donor−acceptor molecular complex by STM. It is found that the intermolecular charge transfer leads to realignment of molecular orbital and the formation of new hybrid highest occupied molecular orbital (HOMO) and lowest unoccupied molecular orbital (LUMO) for the complex, which can be directly visualized by high resolution STM.[28]

Buckyferrocene Fe($C_{60}Me_5$)Cp (Figure 1), in which fullerene and ferrocene are covalently linked through face-to-face

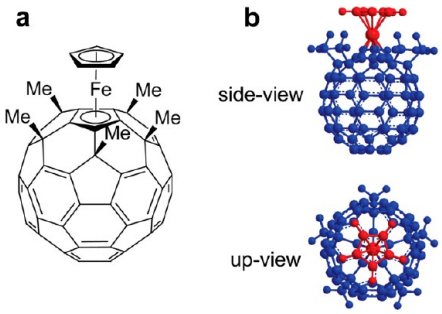

Figure 1. (a) Molecular structure of Fe($C_{60}Me_5$)Cp. (b) Ball-stick models of Fe($C_{60}Me_5$)Cp. For clear resolution, the fullerene moiety and the ferrocene moiety are colored blue and red, respectively.

fusion without any spacing unit, is the simplest fullerene/ferrocene dyad.[29] It is expected to be a suitable model to explore the structure and electron transfer property of electron donor−acceptor dyads for its simple structure and low oxidation potentials. Herein, we investigate the assembly and the electrochemical interfacial electron transfer process of Fe($C_{60}Me_5$)Cp on the Au(111) surface using STM. The electronic structure change of a single molecule, controlled by the interfacial electrochemical electron transfer, is probed by in situ electrochemical STM and supported by theoretical simulations. These experiments provide important information of adstructure and interfacial electron transfer behavior of electron donor−acceptor dyads at the molecular level.

2. EXPERIMENTAL SECTION

All STM experiments were performed using a Nanoscope E STM instrument (Bruker) with a W tip, which was electrochemically etched in 0.6 M KOH and sealed with transparent nail polish to minimize Faradaic currents. All the images were acquired in the constant-current mode to evaluate the corrugation heights of adsorbed molecules.

Au(111) single-crystal surfaces were prepared by the Clavilier method.[30] Before each measurement, the Au(111) electrode was further annealed in a hydrogen−oxygen flame and quenched in ultrapure water (Milli-Q) saturated with hydrogen. Fe($C_{60}Me_5$)Cp was synthesized as per the literatures.[29] To prepare a Fe($C_{60}Me_5$)Cp adlayer, the molecules were dissolved in benzene to form saturated solution. A pretreated Au(111) electrode was immersed in as-prepared benzene solution for several seconds to acquire an Fe($C_{60}Me_5$)Cp monolayer or multilayer. Then the Fe($C_{60}Me_5$)Cp adlayer modified Au(111) surface was mounted in an electrochemical STM cell equipped with two Pt wires as counterelectrode and reference electrode and characterized under potential control. The ex situ cyclic voltammetric measurement was carried out by the hanging meniscus method under a nitrogen atmosphere. A reversible hydrogen electrode with 0.1 M $HClO_4$ as electrolyte (RHE) and a platinum wire were used as reference electrode and counterelectrode, respectively. All the potentials were reported with respect to RHE.

To obtain the dipole moment and molecular orbital of the examined molecule and its cation, the molecule was optimized with density functional theory method at the B3LYP/6-31G* level. All the calculations were carried out with the *Gaussian 09* program.

3. RESULTS

Monolayer of Fe($C_{60}Me_5$)Cp on Au(111) in 0.1 M $HClO_4$ Solution. When a pretreated Au(111) surface is immersed in a benzene solution saturated with Fe($C_{60}Me_5$)Cp for 10 s, a well-ordered monolayer is obtained. Figure 2a is a

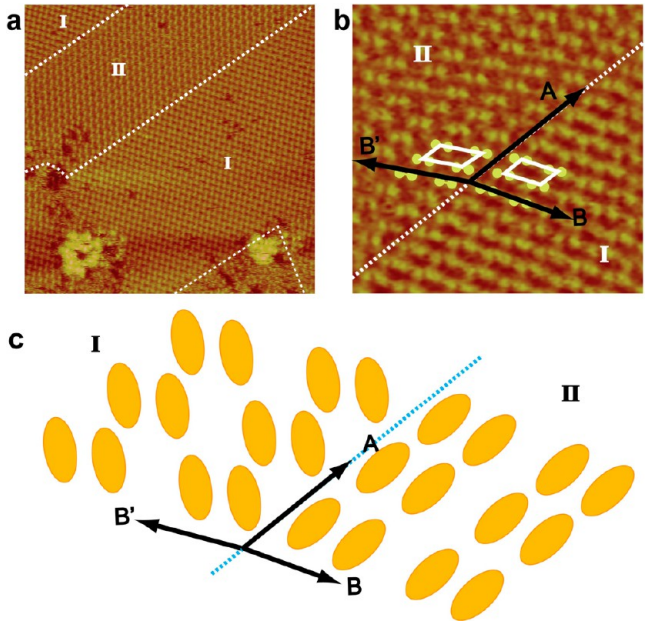

Figure 2. (a,b) Typical STM images of Fe($C_{60}Me_5$)Cp monolayer on Au(111) electrodes in 0.1 M $HClO_4$ solution. Tunneling conditions: (a) scan size = 60 × 60 nm^2, E = 500 mV, E_{bias} = −323 mV, I = 1.129 nA; (b) scan size = 20 × 20 nm^2, E = 500 mV, E_{bias} = −417 mV, I = 984 pA. (c) Proposed structural model of the monolayer.

typical STM image of the monolayer. Well-ordered domains extend to several tens of nanometers with few defects. Careful inspection reveals that two linear structures are contained in the monolayer, named phase I and phase II, respectively. High-resolution STM image shown in Figure 2b gives more details about these two structures. It is revealed that both phases are based upon a set of two spots (illustrated with two linked yellow circles), which acts as the basic structural unit of monolayer. The structural units arrange side by side and form linear patterns. It is clear that the direction of the dimer rows (direction A for both phases) is the same in phase I and phase II, whereas a 10° offset exists between direction B and direction B′, as shown in Figure 2b. Based on above analysis, the unit cells of the two phases are determined, as outlined in Figure 2b. The distances between two structural units within the rows is the same for both phases, i.e. ∼1.6 nm, whereas the distances between neighboring dimer rows (along direction B and B′ in phase I and phase II, respectively) in phase I and phase II have

dx.doi.org/10.1021/ja411813r | J. Am. Chem. Soc. 2014, 136, 3184−3191

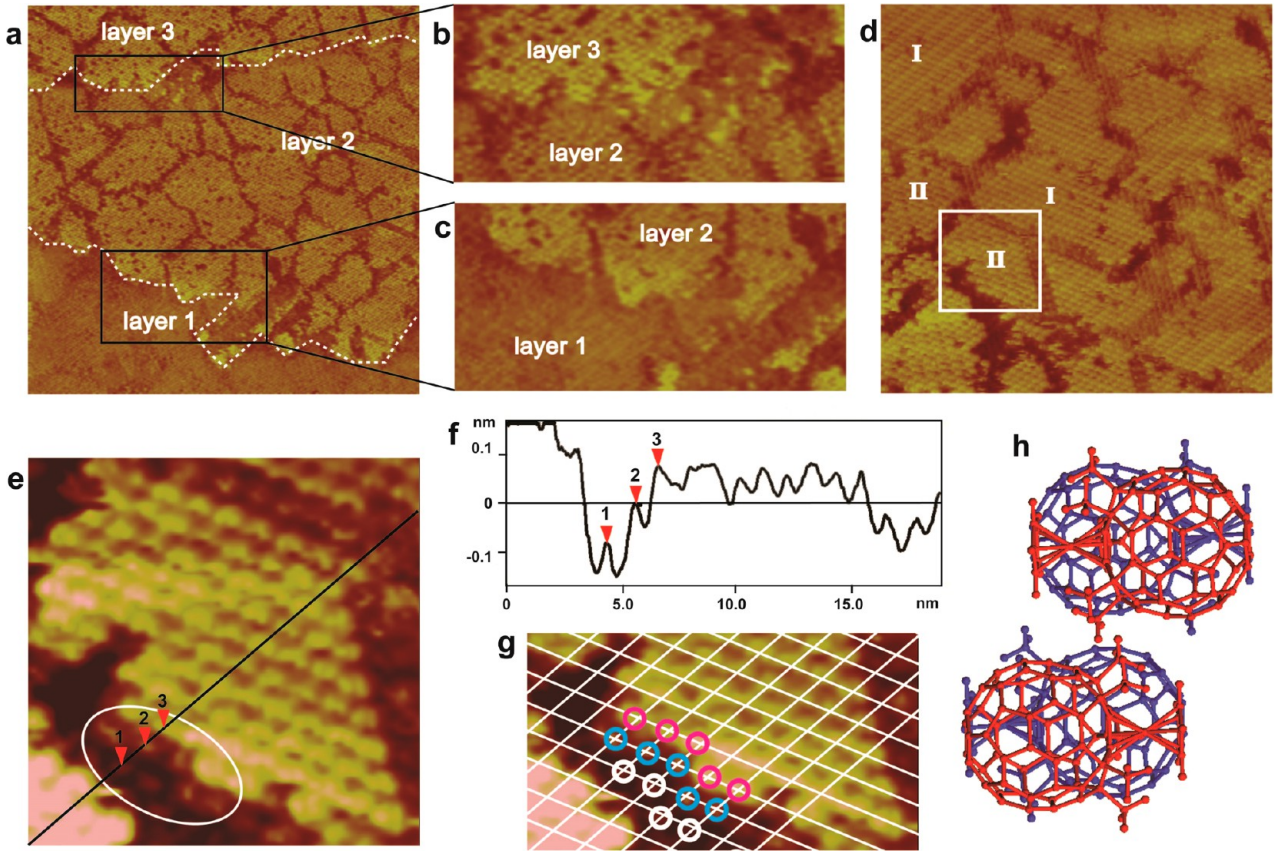

Figure 3. (a–e) Typical STM images of the multilayer formed by Fe($C_{60}Me_5$)Cp on Au(111) electrodes in 0.1 M $HClO_4$ solution. (f) Cross-section profile along the black line in panel e. (g) STM image zoomed from panel e and overlaid with unit cell lattice. (h) Proposed structural model for molecular dimers in the upper layer (colored red) and the lower layer (colored blue). Tunneling conditions: (a) scan size = 130 × 130 nm^2, E = 500 mV, E_{bias} = −300 mV, I = 1.078 nA; (d) scan size = 57 × 57 nm^2, E = 500 mV, E_{bias} = −472 mV, I = 4.727 nA; (e) scan size = 14 × 14 nm^2, E = 500 mV, E_{bias} = −472 mV, I = 4.727 nA.

a tiny difference. The unit parameters for phase I and phase II are $a_1 = 1.6 \pm 0.1$ nm, $b_1 = 2.5 \pm 0.1$ nm, $\alpha_1 = 60 \pm 2°$, and $a_2 = 1.6 \pm 0.1$ nm, $b_2 = 2.8 \pm 0.1$ nm, $\alpha_2 = 50 \pm 2°$, respectively.

The size of each spot is about 0.7 nm, and the distance between two spots within a structural unit is about 1.0 nm. It is inferred that each spot corresponds to an Fe($C_{60}Me_5$)Cp molecule. The structural unit of the adlayer is a dimer of Fe($C_{60}Me_5$)Cp molecule. Furthermore, the distance between two structural units within the molecular row is about 1.6 nm. This distance is so large that a vertical adsorption geometry is unfavored for Fe($C_{60}Me_5$)Cp since molecules always tend to be close-packed to minimize the surface free energy during molecular self-assembly on a solid surface. Thus, the Fe($C_{60}Me_5$)Cp molecule is supposed to adsorb flatly on the surface. Unfortunately, it is difficult to resolve the fullerene moiety and the ferrocene moiety in the STM images. An ellipse is used to represent a lying-flat Fe($C_{60}Me_5$)Cp molecule in the proposed structural model in Figure 2c.

We noticed that the monolayer formed by Fe($C_{60}Me_5$)Cp on Au(111) in 0.1 M $HClO_4$ solution is quite different from that of C_{60} or its analogues.[31−36] For C_{60}, although ordered patterns can be formed on an Au(111) or an Ag(111) surface both in ultra-vacuum and solution environments, the domain size is limited, and many defects exist in the adlayer due to weak intermolecular interactions.[37] In addition, the adlayers of C_{60} and its analogues always display typical six-fold symmetric close-packed structure. The quality of the Fe($C_{60}Me_5$)Cp monolayer has greatly improved so that the size of ordered domains has been amplified and fewer defects are observed. More importantly, the Fe($C_{60}Me_5$)Cp monolayer displays linear structure rather than six-fold symmetry, and its structural unit is an Fe($C_{60}Me_5$)Cp dimer instead of single dispersed molecule. These features imply different interactions in the Fe($C_{60}Me_5$)Cp monolayer compared to adlayers of other fullerenes.

Multilayer of Fe($C_{60}Me_5$)Cp on Au(111) in 0.1 M $HClO_4$ Solution. Prolonging the duration of the Au(111) surface in Fe($C_{60}Me_5$)Cp solution to 30 s, causes a multilayer instead of a monolayer to be obtained, as shown in Figure 3. Three molecular layers, labeled layer 1, layer 2, and layer 3, can be distinguished in Figure 3a. To reveal the feature of multilayer clearly, amplified STM images showing the boundaries between neighboring layers are shown in b and c of Figure 3. The height differences between neighboring layers range from 0.08 to 0.11 nm (the cross-section analysis is shown in Figure S1 in Supporting Information [SI]). The value is significantly different from that of an Au(111) atom step but comparable to the height of a fullerene monolayer,[34,38] suggesting molecular multilayers are acquired by Fe($C_{60}Me_5$)Cp under present experimental conditions. In view of the difficulty to build multilayers of C_{60} on a Au(111) surface in the absence of proper substrate modification in solution environment,[31,33,34] the formation of such multilayers suggests moderate interlayer

dx.doi.org/10.1021/ja411813r | J. Am. Chem. Soc. 2014, 136, 3184−3191

interactions within the assembly of $Fe(C_{60}Me_5)Cp$ in 0.1 M $HClO_4$ solution.

Figure 3d is an STM image with higher resolution. It is clear the uppermost layer also possesses linear structures. To clarify the internal structure of the upper layer, cross-section analysis is performed, as shown in Figure S2, SI. It is suggested that the unit cells of the upper layer and the monolayer agree well. Thus, the molecular arrangement in the upper layer is similar to that in the monolayer. Figure 3e is an amplified image of the area outlined with a white rectangle in Figure 3d. Molecules in different layers can be resolved in the boundary area (highlighted with an ellipse). The brightest spots are molecules in layer 3, the darkest spots correspond to molecules in layer 1, and spots with moderate brightness are molecules in layer 2. The multilayer structure can be observed more clearly in the cross-section profile in Figure 3f.

To further elucidate relative positions of molecules in neighboring layers, Figure 3e is overlaid with the unit cell lattice of molecules in the upper layer, as shown in Figure 3g. The white lines represent the molecular lattice of the uppermost domain, and the white, blue, and red circles denote the molecules in layer 1, layer 2, and layer 3, respectively. It is demonstrated that periodicities in layer 1, layer 2, and layer 3 are the same, indicating molecules in the upper layers also form molecular dimers as building blocks and form linear structures. Moreover, molecules in the upper layer locate almost on the top of the molecules in the lower layer. A possible structural model (Figure 3h) is proposed for molecules in the upper layer and the lower layer, colored red and blue respectively for clear resolution. Molecules within upper layers adopt a lying-flat geometry on the lower layer, too. The C_{60} and ferrocene moieties adopt an antiparallel stacking mode in the neighboring layers to optimize the interactions between them.

Considering C_{60} and ferrocene are electrochemically active, cyclic votammetric measurements were performed on the $Fe(C_{60}Me_5)Cp$ adlayer modified Au(111) electrodes to explore possible electrochemical electron transfer between the molecule and the electrode. However, no obvious redox signal was observed, as shown in Figure S3, SI.

Monolayer of $Fe(C_{60}Me_5)Cp$ on Au(111) in 0.1 M $NaClO_4$ Solution. We next exploit the electrochemistry and ad-structure of $Fe(C_{60}Me_5)Cp$ on Au(111) in 0.1 M $NaClO_4$ solution. Figure 4a is a typical cyclic voltammetric curve of $Fe(C_{60}Me_5)Cp$ adlayer-modified Au(111) electrode in 0.1 M $NaClO_4$ solution. A pair of quasi-reversible redox peaks is observed at ~400 mV and 200 mV for $Fe(C_{60}Me_5)Cp$. Since the reduction of C_{60} occurs at a large negative potential, it is reasonable to ascribe the pair of peaks to the redox of the ferrocene moiety in $Fe(C_{60}Me_5)Cp$. It is noted that the redox potentials are negatively shifted compared to the reported potentials,[29] which may be due to the electrolyte and the working electrode used in the present study being different from those in the literatures.

STM images were first recorded at a substrate potential of 200 mV, ensuring the $Fe(C_{60}Me_5)Cp$ molecule is in the neutral state. Figure 4b shows a typical STM image of $Fe(C_{60}Me_5)Cp$ adlayers on Au(111) in 0.1 M $NaClO_4$ solution. Ordered structures are acquired. The ordered adlayer in 0.1 M $NaClO_4$ solution has a smaller domain size and with more defects than that in 0.1 M $HClO_4$ solution. At the boundary of ordered domains, $Fe(C_{60}Me_5)Cp$ molecules randomly disperse, and some clusters are formed. The ordered $Fe(C_{60}Me_5)Cp$ pattern is unstable and is gradually destroyed and finally becomes

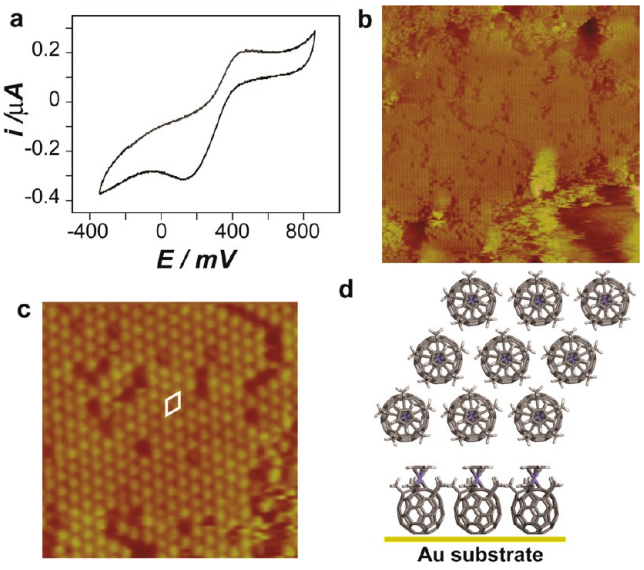

Figure 4. (a) Cyclic voltammetry of $Fe(C_{60}Me_5)Cp$ monolayer on Au(111) electrode in 0.1 M $NaClO_4$ solution. (b, c) Typical STM images of $Fe(C_{60}Me_5)Cp$ monolayer on Au(111) electrodes in 0.1 M $NaClO_4$ solution. Tunneling conditions: (b) scan size = 50 × 50 nm^2, E = 200 mV, E_{bias} = −400 mV, I = 3.168 nA; (c) scan size = 15 × 15 nm^2, E = 200 mV, E_{bias} = −400 mV, I = 3.168 nA. (d) Proposed structural model.

disordered after several scan circles. This phenomenon implies the interaction in the adlayer is relatively weak.

The high-resolution STM image in Figure 4c demonstrates the $Fe(C_{60}Me_5)Cp$ molecule is imaged as a featureless round spot and forms a typical six-fold symmetric close-packed structure in 0.1 M $NaClO_4$ solution. The intermolecular distance is about 1.0 nm, giving a unit cell of a = b = 1.0 ± 0.1 nm and α = 60 ± 2°. This structure is different from the patterns of $Fe(C_{60}Me_5)Cp$ in 0.1 M $HClO_4$ solution but resembles the structure formed by C_{60}.[31,34−37,39] The neighboring molecules are so close that $Fe(C_{60}Me_5)Cp$ cannot lie flat but stands on the substrate. On the basis of previous references, the fullerene derivatives generally adopt adsorption geometry that the fullerene moiety contacts with the solid surfaces.[34,40] Thus, a structural model, i.e. Figure 4d is proposed.

For comparison, we investigate the electrochemical behavior and assembled structure of $Ru(C_{60}Me_5)Cp$, another electron donor−acceptor dyad with structure similar to that of $Fe(C_{60}Me_5)Cp$. No detectable electrochemical signal is observed for $Ru(C_{60}Me_5)Cp$ on Au(111) surface both in 0.1 M $HClO_4$ solution and in 0.1 M $NaClO_4$ solution. Moreover, the typical six-fold symmetric close-packed pattern is formed by $Ru(C_{60}Me_5)Cp$ on Au(111) electrode no matter what molecular concentration and electrolyte is used. Typical STM images and a proposed structural model are shown in Figure S4, SI. The periodicity of the $Ru(C_{60}Me_5)Cp$ adlayer on Au(111) surface resembles that of the $Fe(C_{60}Me_5)Cp$ in 0.1 M $NaClO_4$ solution. Thus, $Ru(C_{60}Me_5)Cp$ molecule is supposed to vertically adsorb and close-pack via intermolecular van der Waals interactions on the Au(111) surface.

Dependence of the $Fe(C_{60}Me_5)Cp$ Structure on the Substrate Potential. We next explore the redox process of the $Fe(C_{60}Me_5)Cp$ adlayer in 0.1 M $NaClO_4$ solution. After the resolution of the assembled structure at the neutral state of $Fe(C_{60}Me_5)Cp$, the substrate potential is set to 500 mV to

dx.doi.org/10.1021/ja411813r | J. Am. Chem. Soc. 2014, 136, 3184−3191

monitor the structure of the oxidized species. It is observed that the structure is nearly unchanged except that most of the molecules become bright in 68 s, as shown in Figure S5, SI. When the substrate potential is set back to the reduction potential, the bright molecules anew become dark very quickly, as shown in Figure S6, SI. It is reported that the dynamic of the reduction (or oxidation) of adsorbed porphyrin is significantly affected by the overpotential applied to the substrate.[41,42] Thus, the substrate potential was positively shifted step by step to study the dependence of the contrast change process upon the overpotential. Figure 5 gives a set of STM images recorded at

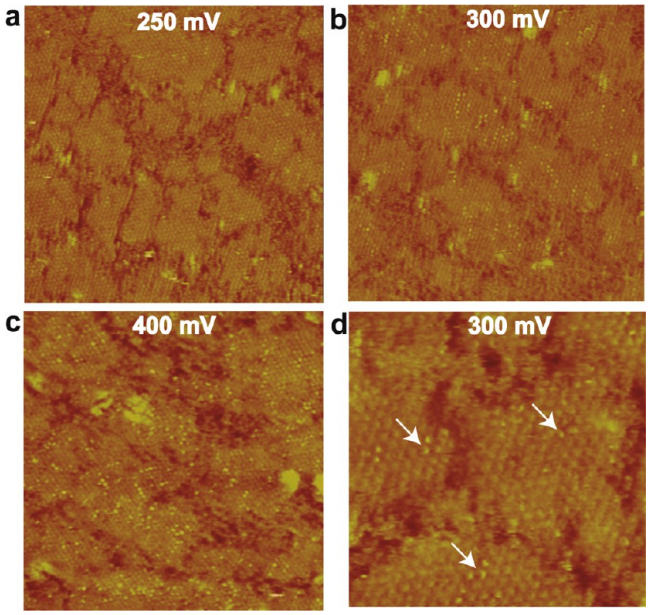

Figure 5. Typical STM images for $Fe(C_{60}Me_5)Cp$ monolayer on Au(111) electrodes in 0.1 M $NaClO_4$ solution. The potentials of the sample are (a) 250 mV, (b) 300 mV, (c) 400 mV, (d) 300 mV. All STM images are shown with the same data scale. Tunneling conditions: (a) scan size = 60 × 60 nm^2, E = 250 mV, E_{bias} = −400 mV, I = 518 pA; (b) scan size = 56 × 56 nm^2, E = 300 mV, E_{bias} = −400 mV, I = 571 pA; (c) scan size = 68 × 68 nm^2, E = 400 mV, E_{bias} = −400 mV, I = 676 pA; (d) scan size = 30 × 30 nm^2, E = 300 mV, E_{bias} = −400 mV, I = 571 pA.

different substrate potentials. As stated above, the $Fe(C_{60}Me_5)$-Cp adlayer in 0.1 M $NaClO_4$ solution is unstable. It is difficult to acquire a series of STM images at one area of the adlayer. STM images in Figure 5 were recorded at a fixed bias potential for the same sample in one experiment but a different area. It can be seen that the six-fold symmetric close-packed structure is sustained during the whole potential range. However, the contrast of some molecules becomes higher when the substrate potential is positive of the molecular oxidation potential. Figure 5a is a typical STM image of the adlayer at 250 mV. No obvious change is observed. All molecules have the same contrast in STM images. When the potential is set to 300 mV (Figure 5b), the onset potential for the oxidation of $Fe(C_{60}Me_5)Cp$, several molecules, about 7% in ratio, become brighter. With further positive shift of substrate potential to 400 mV (Figure 5c), the number of molecules with higher contrast increases. Figure 5d is a high-resolution STM image obtained at 300 mV. Several molecules with higher contrast are marked with white arrows. The size of these brighter spots is inconsistent and far less than 0.7 nm, the theoretical dimension of a C_{60}.

Time Evolution of the $Fe(C_{60}Me_5)Cp$ Adlayer in 0.1 M $NaClO_4$ Solution. In order to examine the time evolution of the $Fe(C_{60}Me_5)Cp$ adlayer in 0.1 M $NaClO_4$ solution, the substrate potential is held at 400 mV. Images a−c of Figure 6 are typical STM images obtained after keeping the electrode at 400 mV for 2.5 min, 12 min, and 40 min, respectively, and images d−f of Figure 6 are their corresponding high-resolution STM images. The number of brighter molecules keeps increasing gradually when the electrode potential is held at 400 mV. The percentage of the brighter spots in the adlayer is about 15% after holding the electrode at 400 mV for 2.5 min. This value increases to 23% when the electrode is kept at 400 mV for 12 min. Images d and e of Figure 6 were recorded at nearly the same area at a 9.5 min interval. Some places are marked for comparison. It can be seen that some dark molecules in Figure 6d become bright in Figure 6e. After being held at 400 mV for 40 min, almost all of the molecules are bright. With the increase of the duration, the bright spots incline to distribute at the ordered domains and form lines, as shown in Figure 6c. It is suggested to result from surface charge diffusion.[41] Electron transfer proceeds more easily between neighboring adsorbed molecules in the ordered domains.

We performed control experiments on $Fe(C_{60}Me_5)Cp$ and $Ru(C_{60}Me_5)Cp$ to elucidate the origin of the STM contrast change. First, the potential dependence of the STM image of $Fe(C_{60}Me_5)Cp$ in 0.1 M $HClO_4$ was studied. No obvious STM contrast change occurs. Then, STM images were recorded for $Ru(C_{60}Me_5)Cp$ at wide potential range in 0.1 M $HClO_4$ and in 0.1 M $NaClO_4$. Neither the six-fold symmetric structure nor the molecular STM contrast changes with the electrode potential within the electrochemical window. This phenomenon is consistent with cyclic voltammetric results which demonstrate no electrochemical reaction occurs for $Fe(C_{60}Me_5)Cp$ in 0.1 M $HClO_4$ or for $Ru(C_{60}Me_5)Cp$ in either 0.1 M $HClO_4$ or 0.1 M $NaClO_4$.

4. DISCUSSION

As a good electron-transfer combination, the conjugation of fullerene and ferrocene is expected to produce large hyperpolarizabilities. Crane et al. prepared the complex of C_{60} and ferrocene in 1982. It is inferred that the hybrid appears to be stabilized by weak intermolecular charge-transfer interactions.[43] Wakahara observed a strong charge-transfer band between ferrocene and C_{60} in C_{60}/ferrocene hybrid hexagonal nanosheets, indicating the presence of donor−acceptor interaction in the nanosheets, and this interaction is supposed to be the driving force for the formation of C_{60}/ferrocene nanosheets.[44] Sawamuraet al.[45,46] prepared directly a covalently linked fullerene/ferrocene dyad. A substantial shift of charge density from the electron donor (i.e., ferrocene) to the electron acceptor (i.e., fullerene) was suggested. We performed theoretical simulations on $Fe(C_{60}Me_5)Cp$ and found obvious dipole moment. The dipole moment is about 6.0 D for $Fe(C_{60}Me_5)Cp$ and points from the ferrocene moiety to the fullerene moiety. This result agrees well with previous reports.[46] It is assumed that the molecular dipole moment is preserved after being deposited on the Au(111) surface, and the dipole−dipole interactions play important roles in the assembly of $Fe(C_{60}Me_5)Cp$. It is assumed that $Fe(C_{60}Me_5)Cp$ molecules adsorb flatly on the substrate and form molecular dimers through dipole−dipole interactions. A structural model of the linear structure is proposed in Figure S7, SI. The molecular dipole within a dimer, both in phase I and phase II, arranges in

dx.doi.org/10.1021/ja411813r | J. Am. Chem. Soc. 2014, 136, 3184−3191

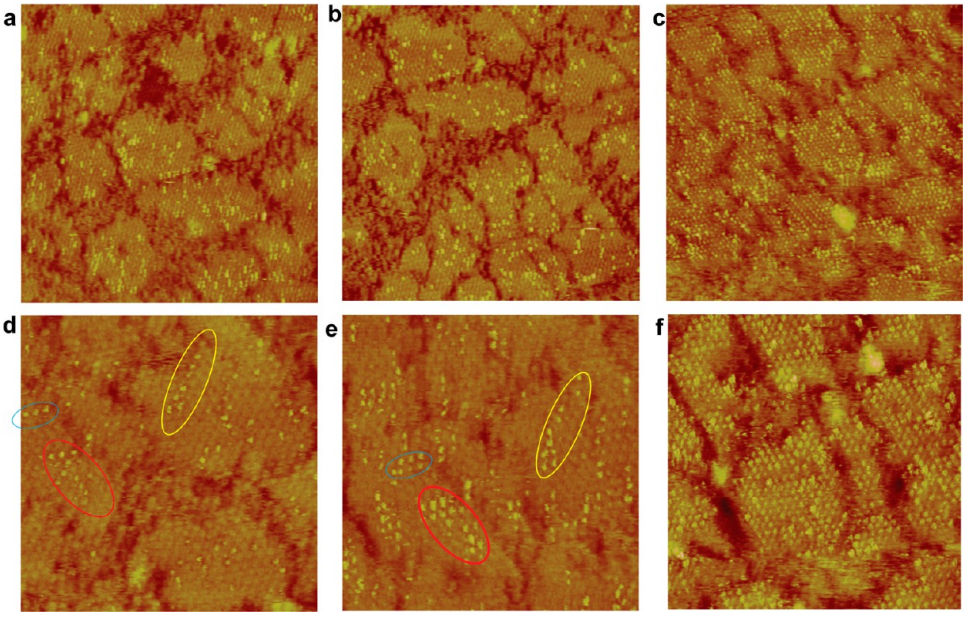

Figure 6. Typical STM images for Fe($C_{60}Me_5$)Cp monolayer on Au(111) electrodes in 0.1 M $NaClO_4$ solution after holding the electrode potential at 400 mV for 2.5 min (a, d), 12 min (b, e), 40 min (c, f). All STM images are recorded at a fixed bias potential and are shown with the same data scale. Tunneling conditions: (a) scan size = 58 × 58 nm^2, E = 400 mV, E_{bias} = −400 mV, I = 518 pA; (b) scan size = 58 × 58 nm^2, E = 400 mV, E_{bias} = −400 mV, I = 518 pA; (c) scan size = 57 × 57 nm^2, E = 400 mV, E_{bias} = −400 mV, I = 606 pA; (d) scan size = 26 × 26 nm^2, E = 400 mV, E_{bias} = −400 mV, I = 676 pA; (e) scan size = 26 × 26 nm^2, E = 400 mV, E_{bias} = −400 mV, I = 676 pA; (f) scan size = 35 × 35 nm^2, E = 400 mV, E_{bias} = −400 mV, I = 550 pA.

an antiparallel mode. This arrangement is energetically favored for intermolecular dipole−dipole interactions.[47,48] Moreover, as revealed by STM images, neighboring molecules in the upper layer and the lower layer also adopt an antiparallel alignment. This arrangement optimizes the dipole−dipole interactions between the neighboring layers and stabilizes the multilayers.

Results of the control experiments about the assembly of the structure of Ru($C_{60}Me_5$)Cp also suggest the formation of the molecular dimer building blocks should be correlated to the molecular dipole moment. As reported, no detectable intramolecular electron transfer occurs in Ru($C_{60}Me_5$)Cp, in both the ground[49] and photoexcited states.[45] Thus, the dipole−dipole interaction in the Ru($C_{60}Me_5$)Cp should be limited, and the van der Waals force is the main intermolecular interaction within the Ru($C_{60}Me_5$)Cp adlayer. As a result, a typical close-packed structure is formed by Ru($C_{60}Me_5$)Cp no matter the molecular concentration and electrolyte used, the same as that observed in the STM images of Ru($C_{60}Me_5$)Cp adlayer on Au(111) electrode in a different electrolyte.

The adsorption and the assembled structure of Fe($C_{60}Me_5$)-Cp on the Au(111) surface are related to the electrochemical environments. The linear structure based on dimer building blocks is only observed for Fe($C_{60}Me_5$)Cp at the 0.1 M $HClO_4$/Au(111) interface but is absent from the adlayer at the 0.1 M $NaClO_4$/Au(111) interface. Moreover, we have explored the adsorption of Fe($C_{60}Me_5$)Cp at the air/solid interface (Figure S8, SI). The Fe($C_{60}Me_5$)Cp molecules randomly disperse on the surface and form a disordered adlayer. This structure is quite different from the structures we observed under the electrochemical conditions. No obvious structural transition is observed for the structure formed in 0.1 M $NaClO_4$ when changing the electrolyte, as shown in Figure S9, SI. It is supposed that the hydration effect and the structure of the electronic double layer may play roles in the different assemblies of Fe($C_{60}Me_5$)Cp in the acidic and neutral electrolytes, although the exact mechanism is unclear. Once one ordered structure is formed, it is difficult to be transformed due to the extra free energy expense for disassembly.

One intriguing phenomenon is that we observed an electrochemically controlled change of the STM contrast of a single Fe($C_{60}Me_5$)Cp molecule in 0.1 M $NaClO_4$ solution. A similar potential-dependent STM contrast change has been reported for other electroactive species.[27,41,42,50−53] For example, He et al. observed that the oxidized 5,10,15,20-tetra(4-pyridyl)-21*H*,23*H*-porphine (TPyP) are dark spots in STM images, while the reduced TPyP are brighter. On this basis, the dynamics of the interfacial electron transfer reaction of TPyP were investigated at the molecular level.[41] Yuan et al. directly visualized the slow electrochemical reduction of adsorbed porphyrin derivative through the difference in the STM contrast between oxidized and reduced states.[42] The origin of the STM contrast change varies. In some cases, it is suggested to be a result of the structural change induced by the charging effect of the electroactive moiety.[53] The difference in the electronic structure of the adsorbate at different potentials may also affect the electron transfer through the molecules. Tsoi et al. demonstrated the electrochemically controlled conductance switching in a quinone-modified oligo(phenylene vinylene). The full bond conjugation in the reduced species provides an efficient, delocalized tunnel barrier for electron transport and results in higher apparent height in the STM image.[27] The dependence of the tunneling current on the overpotential have been demonstrated in many redox active molecules.[54]

In the present study, the STM contrast change is observed for Fe($C_{60}Me_5$)Cp in 0.1 M $NaClO_4$ solution; Fe($C_{60}Me_5$)Cp in 0.1 M $HClO_4$ and Ru($C_{60}Me_5$)Cp in 0.1 M $HClO_4$ or 0.1 M $NaClO_4$ do not show any contrast difference at different substrate potentials. Furthermore, the rate of the dark-to-bright transition is closely dependent on the overpotential applied to

dx.doi.org/10.1021/ja411813r | *J. Am. Chem. Soc.* 2014, 136, 3184−3191

the substrate (Figures 5, and S5, S6 in SI). We ascribe the STM contrast change to the oxidation process of the $Fe(C_{60}Me_5)Cp$ molecule.

Generally, the contrasts and contours of the adsorbate in the STM image are not only determined by the physical shapes of the molecules but are also sensitive to the electronic structure. When the surface adsorbate exhibits electronic state near the Fermi level, the shapes of the molecules in STM images may exhibit the character of individual molecular orbitals, the frontier orbitals in general. We calculated the electron density distribution in the HOMO and LUMO of the neutral $Fe(C_{60}Me_5)Cp$ and the oxidized $Fe(C_{60}Me_5)Cp^+$, as shown in Figure 7. For the neutral species, both the HOMO and the

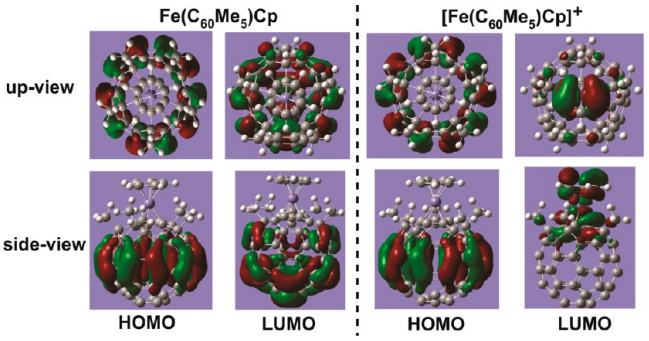

Figure 7. Electron density distributions of the HOMO and LUMO for $Fe(C_{60}Me_5)Cp$ and $Fe(C_{60}Me_5)Cp^+$.

LUMO are mainly located on the fullerene part. Thus, the neutral $Fe(C_{60}Me_5)Cp$ molecule should be a featureless round spot in the STM image, considering the shape of the HOMO and LUMO and its vertical adsorption mode on the Au(111) surfaces, which is consistent with what we observed in the STM measurements. After losing an electron, the HOMO of $Fe(C_{60}Me_5)Cp^+$ is still predominantly located on the fullerene part while the LUMO is mainly positioned on the ferrocene. Since a positive sample bias is used in the STM measurements, the STM image mainly reflects characteristics of the molecular LUMO. The delocalization of LUMO at ferrocene moiety agrees well with the STM image in which smaller and brighter dots are observed. On the basis of the above analysis, it is reasonable to infer that the potential-dependent STM contrast change of $Fe(C_{60}Me_5)Cp$ in 0.1 M $NaClO_4$ should originate from the one-electron electrochemical electron transfer of $Fe(C_{60}Me_5)Cp$ to the Au(111) surface. The electrochemical electron transfer from the molecule to the substrate leads to redistribution of the charge and the realignment of the molecular orbital. As a result, the electronic structure of the molecule changes the LUMO of the molecule so that it is delocalized on the ferrocene moiety. The delocalization can be directly probed by an STM image as the oxidized $Fe(C_{60}Me_5)$-Cp has a higher STM contrast. As a result, we can directly follow the electron transfer process at the molecular level.

The electrochemically controlled variation of the molecular STM contrast cannot result from the adsorption of free molecules onto the molecular adlayer for the following reasons. Generally, the molecules within the bilayer are imaged larger than the molecular size due to the "convolution effect".[55] However, at the onset potential of contrast variation, not the whole molecule but a part of the molecule becomes brighter. Moreover, the $Fe(C_{60}Me_5)Cp$ adlayer was prepared via dipping a pretreated Au(111) electrode in $Fe(C_{60}Me_5)Cp$ solution, and $Fe(C_{60}Me_5)Cp$ is insoluble in aqueous solution. Therefore, the amount of the $Fe(C_{60}Me_5)Cp$ in the aqueous solution is insufficient to give a bilayer.

5. CONCLUSIONS

In summary, we directly probed the assembly and electron transfer of $Fe(C_{60}Me_5)Cp$ onto the Au(111) surface at the molecular level using electrochemical STM supported by theoretical calculations. High-quality monolayer and multilayer are formed by $Fe(C_{60}Me_5)Cp$ on the Au(111) surface in 0.1 M $HClO_4$. $Fe(C_{60}Me_5)Cp$ lies flatly on the Au(111) surface and forms molecular dimers as building blocks. On the contrary, vertical geometry is adopted for $Fe(C_{60}Me_5)Cp$ in 0.1 M $NaClO_4$ solution. Moreover, an electrochemically controlled STM contrast change was observed for $Fe(C_{60}Me_5)Cp$ adlayer in 0.1 M $NaClO_4$. It is supposed to be a result of the delocalization of the frontier orbital originating from the electrochemical electron transfer process. With the loss of one electron, the electronic structure within single $Fe(C_{60}Me_5)Cp$ molecule changes and results in higher contrast in the STM image. The results provide information about the basic structure and property of electron donor–acceptor dyads at the single-molecule level. The in situ STM approach for the investigation of the electrochemical electron transfer process of electron donor–acceptor dyads will benefit the understanding of their structure–function relationship and will provide an experimental basis for the design and preparation of electron donor–acceptor dyad materials.[56,57]

■ ASSOCIATED CONTENT

Supporting Information

Other STM images of the $Fe(C_{60}Me_5)Cp$ adlayer and the contrast change process, cross-section analysis of the multilayers; results of the control experiments, CVs of the Au(111) and $Fe(C_{60}Me_5)Cp$ in 0.1 M $HClO_4$; schematic diagram of the dipole–dipole interactions. This material is available free of charge via the Internet at http://pubs.acs.org.

■ AUTHOR INFORMATION

Corresponding Authors

wangd@iccas.ac.cn
matsuo@chem.s.u-tokyo.ac.jp
wanlijun@iccas.ac.cn

Notes

The authors declare no competing financial interest.

■ ACKNOWLEDGMENTS

This work is supported by National Key Project on Basic Research (Grants 2011CB808700 and 2011CB932300), National Natural Science Foundation of China (Grants 91023013, 21233010, 21121063, 21003131, 20905069, and 21373236), Beijing Municipal Education Commission (20118000101), and the Chinese Academy of Sciences. Y.M. gratefully acknowledges the Funding Program for Next-Generation World-Leading Researchers, and CAS Visiting Professorship Program.

■ REFERENCES

(1) Gayathri, S. S.; Wielopolski, M.; Perez, E. M.; Fernandez, G.; Sanchez, L.; Viruela, R.; Orti, E.; Guldi, D. M.; Martin, N. *Angew. Chem., Int. Ed.* **2009**, *48*, 815.

(2) Mativetsky, J. M.; Kastler, M.; Savage, R. C.; Gentilini, D.; Palma, M.; Pisula, W.; Mullen, K.; Samori, P. *Adv. Funct. Mater.* **2009**, *19*, 2486.

(3) Tkachenko, N. V.; Rantala, L.; Tauber, A. Y.; Helaja, J.; Hynninen, P. H.; Lemmetyinen, H. *J. Am. Chem. Soc.* **1999**, *121*, 9378.
(4) Peeters, E.; van Hal, P. A.; Knol, J.; Brabec, C. J.; Sariciftci, N. S.; Hummelen, J. C.; Janssen, R. A. J. *J. Phys. Chem. B* **2000**, *104*, 10174.
(5) Imahori, H.; Tamaki, K.; Guldi, D. M.; Luo, C. P.; Fujitsuka, M.; Ito, O.; Sakata, Y.; Fukuzumi, S. *J. Am. Chem. Soc.* **2001**, *123*, 2607.
(6) Guasch, J.; Grisanti, L.; Souto, M.; Lloveras, V.; Vidal-Gancedo, J.; Ratera, I.; Painelli, A.; Rovira, C.; Veciana, J. *J. Am. Chem. Soc.* **2013**, *135*, 6958.
(7) D'Souza, F.; Ito, O. *Chem. Commun.* **2009**, 4913.
(8) Guldi, D. M. *Chem. Commun.* **2000**, 321.
(9) Conti, F.; Corvaja, C.; Gattazzo, C.; Toffoletti, A.; Bergo, P.; Maggini, M.; Scorrano, G.; Prato, M. *Phys. Chem. Chem. Phys.* **2001**, *3*, 3526.
(10) Tsuboya, N.; Hamasaki, R.; Ito, M.; Mitsuishi, M.; Miyashita, T.; Yamamoto, Y. *J. Mater. Chem.* **2003**, *13*, 511.
(11) Xenogiannopoulou, E.; Medved, M.; Iliopoulos, K.; Couris, S.; Papadopoulos, M. G.; Bonifazi, D.; Sooambar, C.; Mateo-Alonso, A.; Prato, M. *ChemPhysChem* **2007**, *8*, 1056.
(12) Campidelli, S.; Vazquez, E.; Milic, D.; Prato, M.; Barbera, J.; Guldi, D. M.; Marcaccio, M.; Paolucci, D.; Paolucci, F.; Deschenaux, R. *J. Mater. Chem.* **2004**, *14*, 1266.
(13) Guldi, D. M.; Maggini, M.; Scorrano, G.; Prato, M. *J. Am. Chem. Soc.* **1997**, *119*, 974.
(14) Imahori, H.; Tkachenko, N. V.; Vehmanen, V.; Tamaki, K.; Lemmetyinen, H.; Sakata, Y.; Fukuzumi, S. *J. Phys. Chem. A* **2001**, *105*, 1750.
(15) Hauke, F.; Hirsch, A.; Liu, S. G.; Echegoyen, L.; Swartz, A.; Luo, C. P.; Guldi, D. M. *ChemPhysChem* **2002**, *3*, 195.
(16) Hirayama, D.; Yamashiro, T.; Takimiya, K.; Aso, Y.; Otsubo, T.; Norieda, H.; Imahori, H.; Sakata, Y. *Chem. Lett.* **2000**, 570−571.
(17) Yamada, H.; Imahori, H.; Nishimura, Y.; Yamazaki, I.; Ahn, T. K.; Kim, S. K.; Kim, D.; Fukuzumi, S. *J. Am. Chem. Soc.* **2003**, *125*, 9129.
(18) Roncali, J. *Chem. Soc. Rev.* **2005**, *34*, 483.
(19) Kim, K. S.; Kang, M. S.; Ma, H.; Jen, A. K. Y. *Chem. Mater.* **2004**, *16*, 5058.
(20) Li, S. S.; Northrop, B. H.; Yuan, Q. H.; Wan, L. J.; Stang, P. J. *Acc. Chem. Res.* **2009**, *42*, 249.
(21) Wan, L. J. *Acc. Chem. Res.* **2006**, *39*, 334.
(22) De Feyter, S.; De Schryver, F. C. *Chem. Soc. Rev.* **2003**, *32*, 139.
(23) Li, B.; Li, Z. Y.; Yang, J. L.; Hou, J. G. *Chem. Commun.* **2011**, *47*, 2747.
(24) Lu, Y. H.; Quardokus, R.; Lent, C. S.; Justaud, F.; Lapinte, C.; Kandel, S. A. *J. Am. Chem. Soc.* **2010**, *132*, 13519.
(25) Wasio, N. A.; Quardokus, R. C.; Forrest, R. P.; Corcelli, S. A.; Lu, Y.; Lent, C. S.; Justaud, F.; Lapinte, C.; Kandel, S. A. *J. Phys. Chem. C* **2012**, *116*, 25486.
(26) Ye, T.; Kumar, A. S.; Saha, S.; Takami, T.; Huang, T. J.; Stoddart, J. F.; Weiss, P. S. *ACS Nano* **2010**, *4*, 3697.
(27) Tsoi, S.; Griva, I.; Trammell, S. A.; Blum, A. S.; Schnur, J. M.; Lebedev, N. *ACS Nano* **2008**, *2*, 1289.
(28) Jackel, F.; Perera, U. G. E.; Iancu, V.; Braun, K. F.; Koch, N.; Rabe, J. P.; Hla, S. W. *Phys. Rev. Lett.* **2008**, *100*, 126102.
(29) Sawamura, M.; Kuninobu, Y.; Toganoh, M.; Matsuo, Y.; Yamanaka, M.; Nakamura, E. *J. Am. Chem. Soc.* **2002**, *124*, 9354.
(30) Clavilier, J. *J. Electroanal. Chem.* **1979**, *107*, 211.
(31) Uemura, S.; Sakata, M.; Taniguchi, I.; Kunitake, M.; Hirayama, C. *Langmuir* **2001**, *17*, 5.
(32) Altman, E. I.; Colton, R. J. *Phys. Rev. B* **1993**, *48*, 18244.
(33) Yoshimoto, S.; Narita, R.; Tsutsumi, E.; Matsumoto, M.; Itaya, K. *Langmuir* **2002**, *18*, 8518.
(34) Chen, T.; Pan, G. B.; Yan, H. J.; Wan, L. J.; Matsuo, Y.; Nakamura, E. *J. Phys. Chem. C* **2010**, *114*, 3170.
(35) Wilson, R. J.; Meijer, G.; Bethune, D. S.; Johnson, R. D.; Chambliss, D. D.; de Vries, M. S.; Hunziker, H. E.; Wendt, H. R. *Nature* **1990**, *348*, 621.
(36) Altman, E. I.; Colton, R. J. *Surf. Sci.* **1992**, *279*, 49.
(37) Altman, E. I.; Colton, R. J. *Phys. Rev. B* **1993**, *48*, 18244.
(38) Yoshimoto, S.; Honda, Y.; Ito, O.; Itaya, K. *J. Am. Chem. Soc.* **2007**, *130*, 1085.
(39) Yoshimoto, S.; Narita, R.; Tsutsumi, E.; Matsumoto, M.; Itaya, K.; Ito, O.; Fujiwara, K.; Murata, Y.; Komatsu, K. *Langmuir* **2002**, *18*, 8518.
(40) Yoshimoto, S.; Saito, A.; Tsutsumi, E.; D'Souza, F.; Ito, O.; Itaya, K. *Langmuir* **2004**, *20*, 11046.
(41) He, Y.; Borguet, E. *Angew. Chem., Int. Ed.* **2007**, *46*, 6098.
(42) Yuan, Q.; Xing, Y.; Borguet, E. *J. Am. Chem. Soc.* **2010**, *132*, 5054.
(43) Crane, J. D.; Hitchcock, P. B.; Kroto, H. W.; Taylor, R.; Walton, D. R. M. *J. Chem. Soc., Chem. Commun.* **1992**, 1764.
(44) Wakahara, T.; Sathish, M.; Miyazawa, K.; Hu, C. P.; Tateyama, Y.; Nemoto, Y.; Sasaki, T.; Ito, O. *J. Am. Chem. Soc.* **2009**, *131*, 9940.
(45) Guldi, D. M.; Rahman, G. M. A.; Marczak, R.; Matsuo, Y.; Yamanaka, M.; Nakamura, E. *J. Am. Chem. Soc.* **2006**, *128*, 9420.
(46) Kaji, T.; Shimada, T.; Inoue, H.; Kuninobu, Y.; Matsuo, Y.; Nakamura, E.; Saiki, K. *J. Phys. Chem. B* **2004**, *108*, 9914.
(47) Kudernac, T.; Sandig, N.; Landaluce, T. F.; van Wees, B. J.; Rudolf, P.; Katsonis, N.; Zerbetto, F.; Feringa, B. L. *J. Am. Chem. Soc.* **2009**, *131*, 15655.
(48) Wang, X. Y.; Jiao, T. F.; Zhang, Z. X.; Chen, T.; Liu, M. H.; Wan, L. J.; Wang, D. *J. Phys. Chem. C* **2013**, *117*, 16392.
(49) Matsuo, Y.; Kuninobu, Y.; Ito, S.; Nakamura, E. *Chem. Lett.* **2004**, *33*, 68.
(50) Han, W. H.; Durantini, E. N.; Moore, T. A.; Moore, A. L.; Gust, D.; Rez, P.; Leatherman, G.; Seely, G. R.; Tao, N. J.; Lindsay, S. M. *J. Phys. Chem. B* **1997**, *101*, 10719.
(51) Tao, N. J. *Phys. Rev. Lett.* **1996**, *76*, 4066.
(52) Ye, T.; He, Y. F.; Borguet, E. *J. Phys. Chem. B* **2006**, *110*, 6141.
(53) Yokota, Y.; Miyazaki, A.; Fukui, K.; Enoki, T.; Hara, M. *J. Phys. Chem. B* **2005**, *109*, 23779.
(54) Zhang, J.; Kuznetsov, A. M.; Medvedev, I. G.; Chi, Q.; Albrecht, T.; Jensen, P. S.; Ulstrup, J. *Chem. Rev.* **2008**, *108*, 2737.
(55) Stohr, M.; Wagner, T.; Gabriel, M.; Weyers, B.; Moller, R. *Adv. Funct. Mater.* **2001**, *11*, 175.
(56) Matsuo, Y.; Ichiki, T.; Radhakrishnan, S. G.; Guldi, D. M.; Nakamura, E. *J. Am. Chem. Soc.* **2010**, *132*, 6342.
(57) Lacher, S.; Matsuo, Y.; Nakamura, E. *J. Am. Chem. Soc.* **2011**, *133*, 16997.